Thermo-mechanical fatigue evaluation of a thermal barrier coating bond-coatless system

R. Kromer, F. Mauget, L. Despres, S. Costil, J. Cormier

Thermo-mechanical fatigue evaluation of a thermal barrier coating bond-coatless system

R. Kromer[1*, **], F. Mauget[2], L. Despres[1,2], S. Costil[1], J. Cormier[2]

[1] ICB-LERMPS UMR 6303, Univ. Bourgogne Franche-Comté, UTBM, F-90010 Belfort, France
[2] Institut Pprime - Département de Physique et Mécanique des Matériaux, UPR CNRS 3346, ISAE-ENSMA, Téléport 2, 1, avenue Clément ADER, BP 40109, 86961 CHASSENEUIL – FUTUROSCOPE

*E-mail: robin.kromer@gmail.com
**Now at University of Bordeaux at the institute I2M

Abstract

Thermal barrier coating systems are often subjected to complex thermo-mechanical loading involving a combination of mechanical stresses under complex thermal gradients, in addition to the contribution of oxidation to the damage processes. Recently, a thermal-barrier coating bond-coatless system has been developed using prior-surface treatments. Atmospheric plasma spray (APS) Yttria-Stabilized-Zirconia (YSZ) is deposited on the AM1 nickel-based single crystalline superalloy substrate. The substrate has been either grit-blasted or laser textured before thermal spraying. The durability of these systems are investigated performing out-of-phase load controlled thermo-mechanical fatigue (TMF) tests in the 500 - 1100 °C and 120 - 700 MPa temperature and stress ranges. The contribution of a prior thermal over-aging of 200h at 1100°C has also been investigated. The damage mechanisms during out-of-phase TMF of the different TBC bond-coat-less systems have been studied and compared to the ones obtained during isothermal creep at 1100°C/120 MPa. It is shown that a prior thermal over-aging favors cycling ratcheting during TMF cycling due to the degradation of the substrate microstructure. In addition, the coating damage mechanisms are observed to depend on the prior-surface treatment and thermal over-aging. Cracks perpendicular to the interface in the top coat have been observed whatever the specimens and microstructural state. Top coats are debonded for grit-blasted substrates while crack bifurcation above key holes is observed for laser textured substrates, leading to a better top coat TMF durability.

Keywords: thermal barrier coating, superalloy, γ'-rafting, thermo-mechanical fatigue, thermal-overaging

1 Introduction

Film or wall cooling is widely used in turbine blades employed in the hottest sections of most advanced aero-engines to improve the efficiency of the gas turbine [1]. Moreover, thermal barrier coatings (TBC) are today commonly employed for the design of these components to improve even more the overall efficiency of the gas turbine. TBC systems are usually composed of different layers deposited on a load-bearing superalloy substrate: an alumina-forming metallic bond coat and a ceramic top coat [2]. The bond coat protects the base material from oxidation with thermally grown oxide preferentially of α-Al_2O_3 type and from corrosion. The ceramic top coat is built-up on bond coat using different processes such as EB-PVD or plasma spraying [3]. Prior-surface treatments and bond coats composition are widely studied to enhance adhesion strength and thermal-shock resistance. Nevertheless, premature failure of TBC systems, due to several mechanisms, is still a critical issue from an engine durability point of view [4-7] .

Mechanical anchoring is reported as the main contributor for adhesion in the case of TBC systems [8]. The authors of the present article have hence studied previously laser surface texturing treatment to create thermal barrier coating bond-coat less system (TBC-BCL) [9]. Their recent work showed the benefits of a specific texture on adhesion bond strength, isothermal and thermal cycling oxidation as well as creep resistances. So, the objective of this study is to characterize the degradation mechanisms of this TBC-BCL system under close-to-service conditions, i.e. with changing thermal and mechanical loading paths. The durability and the damage mechanisms of this "new" TBC-BCL system are analyzed under thermo-mechanical loading histories. The understanding of damage development under such conditions requires specific experiments more representative than usual laboratory tests [10]. Within this context, a new testing equipment reproducing service thermo-mechanical loadings of turbine blades profile (mechanical fatigue, thermal fatigue, high heating and cooling rates, hot combustion gases environment, complex thermal gradients) is used [11].

The thermo-mechanical durability of this TBC-BCL has been evaluated in this study using two kinds of prior-surface treatment (i.e. grit-blasting and laser surface texturing) of the substrate. Moreover, two prior-thermal treatments are applied to achieve different microstructure degradation states. First, the paper focuses on the substrate load-bearing capacity under thermo-mechanical fatigue (TMF) tests, considering the intrinsic creep and tensile resistance of the

substrate. Then, thermally grown oxide (TGO) development and coating delamination mechanisms are presented. Finally, the impacts of prior thermal aging and thermo-mechanical cycling are discussed in terms of damage mechanisms.

2 Experimental procedure

2.1 Materials and specimens

Plasma sprayed ceramic top-coat was deposited on the AM1 single crystal superalloy substrate. The AM1 is a first-generation nickel-based single crystal superalloy, whose composition is given in Table 1. Cylindrical specimens was machined out from standard solution heat [12] treated rod supplied by SAFRAN Aircraft Engines, close to a <001> crystallographic orientation (primary misorientation less than 8 degrees), using an electric discharge machining. Cylindrical specimens have been machined for tensile, creep and TMF tests with a total length of 14, 42 and 64 mm and a diameter of 4.0, 3.0 and 4.37 mm respectively. To remove residual stresses induced by machining and to avoid recrystallization during high temperature mechanical tests, specimens were mechanically polished up to a 2000 SiC paper before aging heat treatments (5h/1100°C/AQ + 16h/870°C/AQ) and/or long term over-aging.

2.2 Prior surface treatments

Before spraying of the top coat, theses specimens were surface treated. Grit-blasting (GB) has been used to create a controlled roughness (Ra: 2.3 µm, Rz: 7.8 µm) (Figure 1-a/b). Abrasive-granules have been sprayed with a pressure of 3 bars, at a distance of 5 cm from the surface and using a tangential direction. Laser surface texturing has also been conducted with a pulsed fiber laser (Laseo, Ylia M20, Quantel France) to structure the surface [13]. The laser operated at a nominal wavelength of 1.06 µm with pulse duration of 100 ns, a maximum power of 20 W and variable frequency varying between 10 to 100 kHz. The laser beam used for this operation is circular with a diameter of 60 µm at the focal point and Gaussian energy distribution. Laser patterning consists of series of equidistant lines covered with holes. Patterns with an outer diameter of 80 µm and a depth of 60 µm were made. Holes' depth was limited to 40 µm to optimize ceramic particle spreading during plasma spraying [14]. The distance between patterns has been fixed to 100 µm between revolute center lines (Figure 1-c/d) to maximize adhesion bond strength [15].

2.3 Thermal spraying

The ceramic top-coat has been deposited with atmospheric plasma spraying (F4 torch - Sulzer-Metco - Neuwiesenstrasse 158401 WinterthurSwitzerland) and standard parameters optimized for the TBC material (Table 2). The torch used for top coat deposition is mounted on a XYZ robot to ensure repeatability (ABB robot - Affolternstrasse 44 CH-8050 Zurich Switzerland). Samples turned at 3 revolutions/sec and the torch had a vertical movement of 10 mm/min for homogeneous coating deposition. During the coating deposition, samples were cooled down to room temperature by perpendicularly guided air jets. ZrO_2-$7Y_2O_3$-$1.7HfO_2$ (in wt. Pct) powder (Praxair - ZRO 236-1) has been chosen for the top-coat. The particle size varied from 16 µm to 100 µm ($d_{0.1} - d_{0.9}$) with a 63 µm mean particle size. The top-coat thickness has been evaluated to be 300 ± 12 µm after 12 passes (Figures 1-b and d).

2.4 Prior thermal-aging treatments

Long term annealing of uncoated AM1 specimens has been performed at 1100°C +/- 2°C using a Nabertherm 1800 furnace. Several specimens have been thermally aged up to 300 hours (followed by air quench) to evaluate the evolution of tensile properties at 500°C. Before tensile tests, specimens were carefully polished up to a 4000 SiC paper to remove the γ' depleted and γ' affected layers due to oxidation, in addition to possible local recrystallization of the specimen. A prior over-aging at 1100°C for 200 h has also been carried out before TMF tests using coated specimens. Two TBC-BCL have been studied with and without prior over-aging: grit-blasted and laser textured samples.

2.5 Tensile tests

The substrate mechanical properties have been evaluated by tensile tests at 500°C (+/- 2°C). This temperature is chosen since it corresponds to the lowest temperature applied during out-of-phase TMF tests performed in this study and presented in a subsequent part. The yield stress (taken at 0.2 pct plastic strain offset) has been evaluated with and without a prior thermal-aging (from 24h to 300h at 1100°C). Tension tests have been performed in air using an electromechanical Instron 8562 machine. The strain rate has been fixed to 10^{-3} s^{-1} for all the tests.

2.6 Oxidation analysis

A SETSYS Evolution Atmospheric Thermo-Gravimetric Analysis (TGA) equipment (Setaram, Lyon, France) has been used for thermal cycling oxidation tests. A robust and high performance graphite furnace offering high heating and cooling rates (up to 100 °C/min across the entire temperature range) has been used. The environment used for these tests is synthetic air (20% O_2

and 80% N_2). In this TGA equipment, a symmetrical and hang-down balance detected small mass changes over long term thermal analysis with a precision of +/- 2 µg. The system is used to measure mass uptake/loss during thermal cycling. 100 cycles have been applied to each specimen with ten minutes at 100°C and one hour at 1100°C (see Figure 2). The heating and cooling rates were fixed to 90°C/min. Thermally grown oxides were compared between pure thermal cycling oxidation and TMF tests for TBC-BCL system. Oxide thickness was also evaluated through ten image analysis using the Image J software and specific routines developed for such measurement for each samples [16].

2.7 Creep tests

Creep tests have been performed using a specific set-up developed at Institute Pprime [16]. They are performed under constant load. Heating is ensured by a radiant furnace and plastic strain is measured using a laser beam passing through slots in the furnace. The temperature heterogeneity along the gage length is less than 5°C. Creep tests have been performed using an initial applied tensile stress of 120 MPa at 1100°C. Tests have been stopped at a nearly 1% creep deformation. Non-failed specimens were cooled down to room temperature under load to prevent any stress-free damage development in the TBC system during cooling and any TC spallation.

2.8 Thermo-mechanical fatigue

TMF specimens have been tested using a unique burner rig developed at Institute Pprime (MAATRE burner rig). A burner based on the combustion of natural gas with air supplies hot gases that are blown onto specimens lying in a testing section. These hot gases are accelerated though a convergent exhaust section. Very high heating or cooling rate can be achieved (up to 15°C/s). Temperature and stresses in the specimens have been chosen to obtain a specific cycling with an applied tensile stress of 120 MPa at 1100°C for 1 hour and an applied tensile stress of 700 MPa for 30 seconds at 500°C (Figure 3). Heating and cooling rates were fixed at 10°C/s and temperature was controlled by using a dual wave-length pyrometer in a wavelength range allowing to avoid any variation of emissivity of the top coat [17]. Tests have been stopped when a 3% inelastic strain is reached. The interested reader is referred to [18, 19] for further details regarding the MAATRE burner rig. These out-of-phase (OP) thermo-mechanical fatigue conditions presented in Figure 3 have been chosen to mimic possible loading paths encountered in blades, vanes or shrouds. It is worth mentioning that due to the gas flow around the specimen, the temperature distribution is not homogeneous from the leading edge up to the trailing edge of the specimens. The temperature heterogeneity from the leading edge to the trailing edge, as

measured by different pyrometer measurements, is around 30-40°C during dwell times at maximum temperature (T_{max} at leading edge = 1100°C, T_{max} at trailing edge = 1060-1070°C) while it is nearly 20°C during the low temperature part of our cycle (T_{max} at leading edge = 500°C, T_{max} at trailing edge = 480°C). Along the vertical direction, our temperature distribution is almost homogeneous along the gauge length of our specimen, with a +/- 5°C accuracy. Hence, the temperature profile presented in Figure 3 is the one applied to the leading edge of the specimen and a small temperature gradient across the top coat has been measured during experiments since no internal cooling is applied to the specimens [17]. It is worth mentioning that through post-mortem observations of the γ/γ' microstructure across the section of specimens and subsequent γ' area fraction measurement, no temperature heterogeneity greater than 40°C could have been noticed (not shown here for the sake of clarity). In fact, the γ' fraction is highly sensitive to the local temperature in Ni-based single crystal superalloys for thermal exposure in excess of 1000°C [20-22]. Finally, thanks to specific grips allowing free rotation of the specimens, no induced bending moment is possible in the specimen due to their thermal heterogeneity. A summary of all (thermal-) mechanical and oxidation tests performed in this study is presented in Table 3, as well as a nomenclature of the specimens used.

2.9 Microstructure observations

After tensile, thermal cycling oxidation, creep and TMF tests, specimens have been observed by scanning electron microscopy (SEM). They were cut along the tensile axis (parallel to the <001> axis), then carefully polished and etched using a solution made of 1/3 HNO_3 + 2/3 HCl (volume part) to dissolve the γ'-phase. The microstructure after failure of each specimen has been characterized using JEOL JSM 7000F and JEOL JSM 6400 microscopes operating at 25kV. The different layers of the system have been observed using both the secondary and backscattered imaging modes. In the following of this article, all microstructure observations of TMF specimens have been performed close to their leading edge where the temperature was controlled.

3 Results

3.1 Yield strength evaluation after prior thermal aging treatments

Prior-thermal aging have been performed using uncoated AM1 substrates to evaluate how the high temperature exposure during TMF tests at 1100°C, as well as the prior over-aging of the specimen, may affect yielding during the low temperature part of our OP-TMF cycle. The prior thermal overaging is indeed developed to entail a coarsening of the substrate γ' precipitation and a

decrease of the mechanical properties [23]. Tensile tests have hence been performed to evaluate the evolution of 0.2% Yield strength (Figure 4). In Figure 4, conventional stress has been plotted as a function of the conventional strain.

Increasing the aging time at 1100°C leads to a decrease of the yield stress and tensile strength, from about 1040 to 950 MPa. This decrease is faster during the first 100 hours of exposure and then more sluggish according to Figure 5. Moreover, a decrease in tensile resistance has also been observed (see Table 4).

Microstructure observations have been performed to understand the evolution of tensile properties. Figures 6 and 7 show the microstructural evolution of AM1 single crystal superalloy in the primary dendrite arms and in interdentritic spacings, respectively. After standard solution heat treatment, a regular array of cuboidal γ'-precipitates is observed (Figures 4-a and 5-a). With the increase in thermal exposure at 1100°C, a coarsening of γ'-precipitates is observed. According to different studies, this mechanism is mostly responsible for the degradation of monotonic mechanical properties such as creep and tensile ones [24-27]. Dislocations movements are indeed easier due to a widening of the γ matrix channels and a decrease of the Orowan stress [28, 29]. These results will further be used to analyze the out-of-phase TMF behavior.

3.2 Inelastic behavior during creep and TMF tests

The plastic strain evolutions during creep and OP-TMF tests are presented in Figure 8. All experiments are carried out up to a ~ 3% and ~ 1% inelastic strain for TMF and creep tests, respectively. An insert is provided in Figure 8 to have a better overview on the total creep behavior over all the tests duration.

According to Figure 8, the pure creep behavior is composed of three creep stages; including a small amplitude primary creep stage, a slow secondary creep stage and a very steep tertiary stage. This is a typical creep behavior of high temperature/low stress conditions for Ni-based single crystalline superalloys, i.e. in temperature and stress conditions leading to a fast γ' rafting during the primary creep stage and then, a very slow secondary creep stage [24]. Moreover, the creep time to tertiary creep stage onset is really similar to results obtained by Riallant et al. using the same substrate but with a ~ 75µm thick NiAlPt bond coat and a ~ 160 µm thick EB-PVD YSZ top coat [25]. According to Figure 8, the OP-TMF behavior is also presenting a short primary creep stage. However, no clear stationary creep stage can be observed and an accelerated elongation is observed since ~ 0.3-0.4% plastic strain. It is seen that introducing both thermal and mechanical cycling leads to a faster plastic elongation of the specimens compared to the reference isothermal creep behavior at the conditions used in the hottest part of the TMF cycle.

From Figure 8, the prior over-aging is also shown to decrease the TMF resistance by inducing a higher inelastic strain rate and an earlier acceleration of the plastic strain. Figure 9 shows the isolated strain rates for different cycles of the LST-TMF and LST-TMF-A (cycles 9-10-11 and cycles 30-31-32). Linear interpolations have been performed to evaluate the strain rate during each dwell at maximum temperature during each cycle. Despite slower creep elongation at cycles 9, 10 and 11, it is observed in Figure 8 a steeper increase in strain rate in the over-aged state compared to the LST-TMF specimen. This earlier tertiary stage leads to a shorter time to reach a 3% inelastic strain. Cycles 125-128 have been measured to have almost the same strain rates in LST-TMF specimen as the ones obtained in LST-TMF-A specimen at cycles 9-11. This clearly indicates an earlier onset of tertiary stage in the over-aged state. Plastic deformation also seems to occur during the tensile stage at 500°C due to low temperature mechanical properties modification by the applied prior thermal-aging. Indeed, small amplitude inelastic strain jumps are observed between each cycle, especially toward the end of the tests due to damage accumulation (see LST-TMF-A behavior in Figure 9). The Yield strength and creep degradation due to thermal aging overall result in a lifespan reduction. This last trend is in good agreement with previous OP-TMF results obtained using an EB-PVD TBC system tested using the MAATRE burner rig [17]. It is, however, in apparent contradiction with the OP-TMF behavior observed in CMSX-4 with/without any prior thermal aging at 1000°C by Moverare et al. who observed almost no effect of the prior over-aging [30]. Indeed, in their case, since experiments were performed in strain-controlled mode, a relaxation of the minimum stress was obtained during compressive dwell at high temperature. Since the prior over-aging favors such a stress relaxation process, lower (in magnitude) compressive stresses were obtained in the over-aged state in their case, overall leading to higher tensile stresses and larger plastic strain in the cold part of their TMF cycle. This greater stress relaxation in the hot part of their TMF cycles was hence couter-balanced by greater yielding in the cold part of their cycle, overall leading to similar TMF lives with and without any prior over-aging. Besides, the prior-surface treatments hardly affect creep or OP-TMF behavior and durability in the investigated conditions.

The substrate microstructure in the as-received state and after creep/OP-TMF tests is shown in Figure 10. A classical γ/γ' microstructure is observed before testing, with γ' cuboidal particles having a 0.4-0.5 µm edge length (Figure 10-a). A rafted γ/γ' microstructure is established at the end of creep and TMF tests (Figure 10-b; 10-cand 10-d), whether a prior over-aging is applied or not. As a main consequence of the prior over-aging of 200h at 1100°C, and despite a shorter

TMF tests, thicker γ'-rafts are obtained (see Figure 10-d) compared to pure creep (Figure 10-b) or OP-TMF tests without any prior aging (Figure 10-c). This is clear indication that most of the coarsening of the γ'-phase had already developed during the prior thermal exposure. One may also notice in Figure 10-d γ'-rafts not perpendicular to the tensile stress axis, which is another indication that most of the microstructure degradation took place during the prior 200h thermal exposure at 1100°C before OP-TMF tests, in good agreement with Figures. 6 and 7.

3.3 TGO growth under thermal cycling and thermomechanical conditions

The exact parameters governing TBC systems lifetime during high-temperature service are still subject to debate. It is generally accepted that the growth rate, morphology, cristallography and adherence of the aluminum-based thermally grown oxide scale (TGO) which forms during high-temperature service is of crucial importance for the eventual occurrence of top coat spallation [31]. Upon first exposure at a high temperature, i.e., during heat treatment, the system tends to form different types of oxides, e.g. Cr_2O_3, NiO, $(Ni,Co)(Cr,Al)_3O_4$ etc. [9]. The transition of this heterogeneous scale into a stable α-Al_2O_3-based layer can lead to stress initiation and/or result in the formation of cracks which may be further crack initiation sites during high temperature service, especially under thermal cycling conditions [32]. Figure 11 shows that the TGO after OP-TMF tests is composed of two grey layers (light and dark) corresponding to spinel (outer layer) and alumina oxides (inner layer) respectively [33].

According to Figure 12, the relative mass uptake during thermal cycling oxidation is rather similar for both type of specimens (i.e. grit blasted or laser textured) despite differences in the surface morphology and preparation. A typical parabolic growth has been observed for both types of specimens with only noticeable differences within the transient regime at the beginning of oxidation tests.

TGO thickness has been measured after mechanical tests for the different samples and compared to the oxide thickness after pure thermal cycling oxidation (Table 5). The TGO is in fact thicker after OP-TMF cycling than after pure thermal cycling conditions. This may result from possible TGO cracking in the low temperature part of the TMF cycle (i.e. below 700°C) due to both a brittle character of the oxide scale and the superposition of a large tensile stress [34]. We believe that given the high heating and cooling rates used during both type of experiments (1.5°C/s in thermal cycling oxidation versus 10°C/s during OP-TMF tests), a direct contribution of thermal transients in terms of TGO thickening can be neglected.

3.4 Top coat damage mechanisms under TMF conditions

After a macroscopic overview, vertical cracks are observed in the top coat of TMF specimens after 3% plastic deformation, whatever the prior surface treatment. The surface density of micro-cracks is equal to 31, 46 and 78 cracks per meter for GB-TMF, LST-TMF and LST-TMF-A respectively. These cracks results from the lack of (plastic) strain tolerance of this kind of plasma sprayed top coat during cyclic thermo-mechanical loading [10]. Furthermore, t based on the crack density, some assumptions on the top coat adhesion can be performed. Indeed, a high crack density suggests a good adhesion of the ceramic top coat, since the metallic substrate imposes its total strain (i.e. elastic, thermal and plastic strain) to the coating. Figure 13 suggests that the coating followed the substrate inelastic deformation until the nucleation and propagation of vertical cracks in the top coat. These vertical cracks then deviated near the top coat/substrate interface. Their number can then be attributed to the number of cycles up to complete delamination of the top-coat [35].

Having a closer look at the crack bifurcation, it is seen from Figure 13(a) that either cracks follow the TC/substrate interface and/or inter-splat/oxide defects for grit-blasted samples. Also cracks are deviated above holes for laser textured specimens. Cracks nucleated within the thickness of the top coat then have propagated above the interface for LST-TMF (Figure 13(b)). Cracks have also propagated above holes for LST-TMF-A (Figure 13(c)) and followed pattern edges. Besides; vertical micro-cracks cracks are observed in hole for prior-thermally exposed specimens (Figure 11(b)). Interface cracks were only observed for grit-blasted sample after creep tests.

According to previous figures, prior-surface treatments affect the coating delamination mechanisms. Top coats remained trapped on the substrate in case of laser surface texturing, then forcing crack deviation above the TC/substrate interface. The patterns could then be defined as crack propagation obstacles. Finally, it is worth noting that no crack is observed to initiate from key holes introduced in the substrate after a 3% plastic strain during burner rig OP-TMF tests. This result is in agreement with a similar observation in isothermal creep in a previous article from the authors [9] in which no cracks are observed after a 1% creep strain starting from key holes. This substrate surface morphology introduced by laser texturing hence does not seem to favor crack initiation during high temperature monotonous and thermo-mechanical loading.

4 Discussion

The TMF durability of a bond coatless TBC system has been investigated in simulated gas turbine environment using the MAATRE burner rig. In the following, the effect of thermo-

mechanical cycling on the overall system mechanical resistance to inelastic deformation and the TC/substrate interface evolution during TMF cycling will be discussed.

4.1 Microstructure evolution under TMF

The discussion first focuses on the strain rate comparison between TMF and creep tests. TMF tests are composed of a high-temperature stage (+120MPa/1100°C) and a low-temperature tensile stage (+700MPa/500°C) with two fast temperature transitions (cooling and heating). This thermo-mechanical cycle induces microstructure evolutions during each cycle and leads to a faster strain rate compared to pure isothermal creep conditions under the same conditions of the high temperature stage of the TMF cycle (see Figure 13). When LST-TMF and LST-Creep strain rates are compared in Figure 14, a nearly one order of magnitude difference is observed after 20 hours of test. This result is quite in good agreement with Arrell et al. study on the impact of the prior substrate microstructure degradation on the number of cycles to crack initiation in TMF in CMSX-4 alloy [36]. However, in our case, we have decided to stop our OP TMF tests at a nearly 3% inelastic strain to avoid any contribution of macroscopic crack propagation within the substrate to the overall behavior. As such, a direct comparison between isothermal creep and TMF behaviors is possible, with a very limited contribution of damage in the form of cavitation or crack propagation [17, 28, 37].

First, it was shown by Raffaitin et al. that introducing a thermal cycling in the creep life at 1150°C/80 MPa of MC2 Ni-based SX alloy leads to a faster strain rate and lower creep life [38]. In their study, the creep strain at the end of the primary creep seems to be independent of the type of creep test for a given applied stress. Finally, the difference between the two types of creep tests lied essentially in the duration of the steady-state stage, which is responsible of the difference in high-temperature creep lifetime. A reduction in high-temperature creep life associated with thermal cycling was clearly evidenced, this reduction being greater for a higher cycling frequency. A similar trend has also been observed by Giraud et al. and then by Cormier during thermal cycling conditions involving repeated overheatings [39, 40]. According to Cormier, creep resistance under non-isothermal conditions is primarily controlled by the remaining γ' volume fraction at high temperature, whatever the thermal cycling type [41,16]. The dissolution of the coherent γ' precipitates and their subsequent re-precipitation on cooling affected the mechanical behavior of the alloy and the creep lifetime [16]. Moreover, and as a main result from le Graverend et al. in situ investigation by X-Ray diffraction under synchrotron beam of the creep behavior [42], the observed faster strain rate under thermal cycling creep conditions compared to pure isothermal conditions results from the easier penetration of dislocations with γ'-precipitates,

a result that has been confirmed recently by Schwalbe et al. by TEM investigations [43]. The thermal cycling applied during our TMF conditions is then probably responsible for an important increase of the creep rate, which leads to a decrease in lifetime at high temperature. Moreover, the large tensile stress (+700 MPa) applied at 500°C, even if below the Yield stress defined at a 0.2% plastic offset according to Figures 4 and 5, may also favor precipitate shearing toward the end of the test in a very localized way, due to the degradation of the γ/γ' microstructure. It is indeed well known that first slip bands at low temperatures (i.e. below 600°C in high γ' volume fraction containing Ni-based superalloys) may emerge at applied stresses far below the 0.2% macroscopic stresses [44, 45].

The impact of the prior over-aging at 1100°C on the OP TMF resistance is more straightforward since the prior microstructure degradation is not only shown to induce a debit in tensile properties at 500°C (see Figure 4 and Table 4), but also a decrease of the creep properties. Indeed, according to Mauget et al. [17], Steuer et al. [27], Riallant [46] and Shi et al. [23], a prior microstructure coarsening leads to a faster strain rate due to wider γ-channels and hence, easier dislocation by-passing mechanisms due to a lower Orowan stress. According to the TMF behaviors shown in Figures 8 and 9, the effect of the prior over-aging of 200h at 1100°C on the creep resistance at 1100°C has a prominent contribution to the faster inelastic strain rate rather than the loss of Yield stress at 500°C since inelastic strain jumps during temperature/stress transients only occur toward the end of the tests. Indeed, the Yield stress at 0.2% is of nearly 965 MPa at the beginning of TMF test, i.e. far above the applied tensile stress of 700 MPa. Yielding at 500°C during TMF tests using pre-aged specimens only occur once the microstructure has sufficiently coarsened (see Figure 10(d)). The only unexplained result from the present study is the very low minimum inelastic strain rate observed during TMF tests using pre-aged specimens (see Figure 13). This minimum inelastic strain rate, reproducible for both grit-blasted and laser textured specimens, is even lower that the minimum creep rate observed in pure isothermal conditions. A possible reason for this unexpected minimum strain rate could be the re-orientation of γ/γ' interfaces during TMF tests since a non-directional coarsening has been obtained after the prior exposure of 200h at 1100°C (see Figures 6(d) and 7(d)) while a directional coarsening tends to operate during our TMF tests since a tensile stress is kept applied during all our tests. Such interfaces re-orientation was already observed by Giraud et al. [39] and by Xingfu et al. [47] during high temperature creep tests with a prior pre-rafting in compression. This assumption needs to be checked in the future by performing interrupted experiments.

4.2 Interface evolution under TMF

In all the experiments presented in this article, the top-coat followed the substrate deformation during TMF and creep experiments. The inability of the APS coating to recover to its original dimensions during cooling causes in-plane biaxial tension in the coating. When the tensile stresses exceed the fracture strength of the newly sintered and compacted YSZ, the energy is relieved by through-thickness crack growth and possible delamination of the coating at the interface [48]. Petorak et al. proposed an explanation of compressive stress relaxation in APS coatings, which is proportionally linked to the magnitude of tensile stress with rearrangement and sliding of lamella [49]. The coating lamellar structure has a poor plastic strain tolerance compared to EB-PVD processed top coat, overall leading to vertical cracks after a ~ 1% plastic strain has been reached [50].

For grit-blasted specimens, an entire delamination of the top coat is observed and a full spallation has been obtained soon after the end of the TMF tests. The buckling mechanisms are known to be favored for a grit-blasted substrate by the cyclic applied stresses [34] and very sudden spallations have been observed during cooling stages of TMF tests by other groups due to the stress state in each layer of the TBC system [51, 52]. In our case, no ductile-brittle transition of a bond-coat can be invoked for such a top coat spallation since no bond-coat is used, but the stress distribution during cooling across the top coat and substrate, in addition to the substrate roughness after grit blasting are enough to favor interfacial delamination compared to texture specimens.

For textured specimens, crack deviation has been observed above the patterns. These deviations can be a result of compressive stresses in the vicinity of holes which enable crack bifurcation and hence, better durability of the top coat. The interested reader is referred to a previous article form the authors regarding the better durability in thermal oxidation resistance of laser texture specimens [9]. Two distinct damage behaviors are observed for LST specimens after TMF tests (see Figure 12). LST-TMF has crack deviations above holes and no crack propagating toward the substrate could have been observed. However, for LST-TMF-A specimens, vertical cracks propagating toward the substrate have been detected, coming from the top coat (see Figure 11(b)). These cracks have reached the γ′-depleted layer in the bottom of hole. This first cracks identified to propagate from the top coat tower the substrate probably result from the larger γ′-depleted layer below the substrate/top coat interface due to the prior over aging, this layer having a worse resistance to crack propagation. It is anticipated that by increasing the duration of our

TMF tests, by, e.g., lowering the applied stress at 1100°C, such cracks may also develop in LST-specimens for longer TMF testing time.

Kyaw et al. demonstrated by finite element simulation that tensile stresses are predicted to be concentrated at the near-interface peaks during heating. The stresses near these cracks relax while their propagation towards the valley region is opposed by high compressive stress [53]. After the heating stage, stress reversal at the TBC peak and valley regions does not occur rapidly, specifically for the aged system with thick initial TGOs compared to the as-sprayed system. Shalka et al. showed also that cracks nucleate at the TBC peak during heating continue to propagate during the steady state heating stage for aged systems and premature spallation is expected [54]. During steady state heating, additional parallel cracks are expected to nucleate at the TBC valley due to stress reversal at the TBC peak and valley. When cooling is applied, any thermal expansion mismatch is predicted to cause tensile out-of-plane stresses in the vicinity of the peak and the valley and slope of the TBC. The authors assume that at the end of cooling, tensile delamination cracks are expected to occur at the peak near the interface interface. TGO for aged samples can also be identified as a crack nucleation and strain could drive micro-cracks and nucleate with further propagation of existing TBC.

5. Conclusions

The Out-of-Phase TMF behavior of a new thermal barrier coating bond-coat less system (ceramic top-coat + single crystal nickel-based superalloy) has been studied in a simulated gas turbine environment. The applied TMF cycle was composed of 1 hour at 1100°C/+120 MPa + 30 seconds at 500°C/+700 MPa. From this work, the following main conclusions can be established

- The Out-of-phase thermo-mechanical cycling increased the inelastic strain rate compared to the pure isothermal creep reference in the conditions of the high temperature part of the TMF cycle. This faster plastic strain rate results mainly from a faster creep rate on each dwell at 1100°C due to the temperature cycling. This temperature cycling indeed favors faster coarsening of the γ'-phase as well as easier penetration of dislocations in γ'-precipitates.
- Prior thermal over-aging for 200h at 1100°C induces a coarser γ/γ' microstructure which promoted faster creep elongation at 1100°C and lower yield stress at 500°C. The TMF resistance is then lower after introducing a prior thermal over-aging.

- Prior-surface treatments (either grit blasting or laser texturing) did not weaken this TBC system by favoring crack initiation from holes or a recrystallized layer below the surface.
- Laser surface texturing of the substrate leads to crack deviation above the interface. The cavities introduced in the substrate are inducing coating compressive stresses and can be defined as obstacles for top coat crack propagation.

Acknowledgement

The authors gratefully acknowledge the French Research Agency ANR for financial assistance in the ARCOLE (12-BS09-0009) project. A part of this study is conducted in the framework of the LABEX INTERACTIFS at Institute Pprime UPR CNRS 3346 under contract number ANR-11-LABX-0017. SAFRAN Aircraft Engines is gratefully acknowledged for providing AM1 single crystalline bars.

References

[1] X. Q. Cao, R. Vassen, and D. Stoever, “Ceramic materials for thermal barrier coatings,” *J. Eur. Ceram. Soc.*, vol. 24, no. 1, pp. 1–10, 2004.
[2] D. R. Clarke and S. R. Phillpot, “Thermal barrier coating materials,” *Mater. Today*, vol. 8, no. 6, pp. 22–29, 2005.
[3] R. Eriksson, S. Sjostrom, H. Brodin, and S. Johansson, “Article - R.Eriksson - TBC bonding coat top coat interface roughness.pdf,” *Surf. Coat. Technol.*, no. 51, 2013.
[4] J. Allen Haynes, E. Douglas Rigney, M. K. Ferber, and W. D. Porter, “Oxidation and degradation of a plasma-sprayed thermal barrier coating system,” *Surf. Coat. Technol.*, vol. 86, pp. 102–108, 1996.
[5] R. D. Jackson, “The effect of bond coat oxidation on the microstructure and endurance of two thermal barrier coating systems,” PhD Thesis, University of Birmingham, 2010.
[6] K. Al-Athel, K. Loeffel, H. Liu, and L. Anand, “Modeling decohesion of a top-coat from a thermally-growing oxide in a thermal barrier coating,” *Surf. Coat. Technol.*, vol. 222, pp. 68–78, 2013.
[7] D. Balint and J. Hutchinson, “An analytical model of rumpling in thermal barrier coatings,” *J. Mech. Phys. Solids*, vol. 53, no. 4, pp. 949–973, 2005.
[8] C. C. Berndt, “Tensile Adhesion Testing Methodology for Thermally Sprayed Coatings,” *J. Mater. Engineeing*, vol. 12, pp. 151–158, 1990.
[9] R. Kromer, J. Cormier, S. Costil, D. Courapied, L. Berthe, P. Peyre "High temperature durability of a bond-coatless plasma-sprayed thermal barrier coating system with laser textured Ni-based single crystal substrate," *Surf. Coat. Technol.*, vol. 337, pp. 168-176, 2018.
[10] S. R. Choi, D. Zhu, and R. A. Miller, “Fracture behavior under mixed-mode loading of ceramic plasma-sprayed thermal barrier coatings at ambient and elevated temperatures,” *Eng. Fract. Mech.*, vol. 72, no. 13, pp. 2144–2158, 2005.
[11] J. Cormier, F. Mauget, J.B. le Graverend, C. Moriconi, J. Mendez, "Issues related to the constitutive modeling of Ni-based single crystal superalloys under aeroengine certification conditions," *J. AerospaceLab,* Vol. 9 , 2015.

[10] A. Moridi, M. Azadi, and G. H. Farrahi, “Thermo-mechanical stress analysis of thermal barrier coating system considering thickness and roughness effects,” *Surf. Coat. Technol.*, vol. 337, pp. 168-172, Mar 2018.
[11] D. Jun, H. Xia, C. Song, and Y. E-Chuan, "Numerical Simulation Procedure for Modeling TGO Crack Propagation and TGO Growth in Thermal Barrier Coatings upon Thermal-Mechanical Cycling," *Adv. Mater. Sci. Eng.*, vol. 2014, pp. 1–14, 2014.
[12] L. Rougier, A. Jacot, C.A. Gandin, P.D. Napoli, D. Ponsen, V. Jaquet, "Numerical simulation of AM1 microstructure," *MATEC Web of Conferences Eurosuperalloys,* vol. 14, 11003, 2014.
[13] R. Kromer, S. Costil, J. Cormier, L. Berthe, P. Peyre, and D. Courapied, “Laser Patterning Pretreatment before Thermal Spraying: A Technique to Adapt and Control the Surface Topography to Thermomechanical Loading and Materials,” *J. Therm. Spray Technol.*, vol. 25, no. 3, pp. 401–410, 2016.
[14] R. Kromer, S. Costil, J. Cormier, D. Courapied, L. Berthe, P. Peyre, and M. Boustie, “Laser Surface Patterning to enhance adhesion of Plasma Sprayed Coatings Surface and Coatings Technology.” *Surf. Coat. Technol.*, vol. 352, pp. 642-653, 2017.
[15] R. Kromer, J. Cormier S. Costil, " Role of Powder Granulometry and Substrate Topography in Adhesion Strength of Thermal Spray Coatings, " *J. Therm. Spray Technol.*, vol. 25, no 5, pp.933-945, 2016.
[16] J. Cormier, "Thermal Creep Resistance of Nickel Based Single Crystal Superalloys," *Superalloys conference,* at Seven Springs, PA, USA, edit TMS, 2016.
[17] F. Mauget, F. Hamon, M. Morisset, J. Cormier, F. Riallant, J. Mendez, "Damage mechanisms in an EB-PVD thermal barrier coating system during TMF and TGMF testing conditions under combustion environment," *Intern. J. of Fatigue*, vol.99, pp.225-234, 2017.
[18] F. Mauget, D. Marchand, G. Benoit, M. Morisset, D. Bertheau, J. Cormier, " Development and use of a new burner rig facility to mimic service loading conditions of Ni-based single crystal superalloys, " *MATEC Web of Conferences Eurosuperalloys,*" vol.14, 20001, 2014.
[19] F. Mauget, D. Marchand, M. Morisse, D. Bertheau, J. Cormier, J. Mendez, " Nouveau moyen de caractérisation des matériaux: Conditions extrêmes et sollicitations thermomécaniques proches des conditions d’usages," *Matériaux Tech*, vol. 6, no. 7, pp. 541–545, 2012.
[20] J. Cormier, X. Milhet, J. Mendez, " Effect of very high temperature short exposures on the dissolution of the γ′ phase in single crystal MC2 superalloy, " *Materials science,* vol. 42, no. 18, pp. 7780-7786, 2007.
[21] R. Giraud, Z. Hervier, J. Cormier, G.Saint-Martin, F. Hamon, X. Milhet, J. Mendez, "Strain Effect on the γ′ Dissolution at High Temperatures of a Nickel-Based Single Crystal Superalloy, " *Metallurgical and Materials Transactions A*, vol. 44, no. 1, pp.131-146, 2013.
[22] C.Swalbe, A. Jaques, E. Galindo-Nava, C.N. Jone, C.M.F. Rae, J. Cormier, " In situ measurement of the precipitate volume fraction and interfacial lattice misfit during non-isothermal creep in the superalloy CMSX-4, " *Materials Science and Engineering A*, vol. 740-741, pp.182-186, 2019.
[23] Z.Shi, J. Li, S. Liu, "Effect of long term aging on microstructure and stress rupture properties of a nickel based single crystal superalloy, " *Progress in Natural Science: Materials International*, vol. 22, pp. 426-432, 2012.
[24] R.C. Reed, N. Matan, D.C. Cox, M.A. Rist, C.M.F. Rae, " Creep of CMSX-4 superalloy single crystals: effects of rafting at high temperature, " *Acta Materialia,* vol. 47, no. 12, pp. 3367-3381, 1999.

[25] F. Riallant, J. Cormier, A. Longuet, X. Milhet and J. Mendez, "High temperature creep degradation of the AM1/NiAlPt/EBPVD YSZ system, " *Metallurgical and Materials Transactions A*, vol. 45, no. 1, pp.351-360, 2014

[26] M. Aghaie-Khafri, M. Hajjavady, The effect of thermal exposure on the properties of a Ni-base superalloy, *Materials Science and Engineering A*, vol. 527, pp. 890–897, 2010.

[27] J.L. Liu, T. Jin, J.J. Yu, X.F. Sun, H.R. Guan, Z.Q. Hu, Effect of thermal exposure on stress rupture properties of a Re bearing Ni base single crystal superalloy, *Materials Science and Engineering A,* vol. 527, 890–897, 2010.

[28] S. Steuer, Z. Hervier, S. Thabart, C. Castaing, M. Pollock, J. Cormier, " Creep behavior under isothermal and non-isothermal conditions of AM3 single crystal superalloy for different solutioning cooling rates, " *Materials Science and Engineering A*, vol. 601, pp. 145-152, 2014.

[29] R.Desmorat, A.Mattiello, J.Cormier, "A tensorial thermodynamic framework to account for the gamma' rafting in nickel-based single crystal superalloys, "*Intern. J. of Plasticity*, vol. 95, pp. 43-81, 2017.

[30] J. J. Moverare, S. Johansson, R.C. Reed, "Deformation and damage mechanisms during thermal–mechanical fatigue of a single-crystal superalloy, " *Acta Materialia,* vol. 57, no. 7, pp. 2266-2276, 2009.

[31] W.J. Quadakkers, V. Shemet, D. Sebold, R. Anton, E. Wessel, L. Singheiser, " Oxidation characteristics of a platinized MCrAlY bond coat for TBC systems during cyclic oxidation at 1000°C, " *Surface & Coatings Technology,* vol.199, pp. 77– 82, 2005.

[32] A. Vande Put, D. Oquab, A. Raffaitin, D. Monceau, " Influence of Pt Addition and Manufacturing Process on the Failure Mechanisms of NiCoCrAlYTa-Base Thermal Barrier Coating Systems under Thermal Cycling Conditions, " *Metals*, vol. 8, no. 771, 2018.

[33] R.Kromer, "Etude des effets des préparations de surface avant projection thermique : application barrière thermique, "PhD Thesis, UTBM, 2016.

[34] A.G. Evans, D.R. Mumm, J.W. Hutchinson, G.H. Meier , F.S. Pettit, "Mechanisms controlling the durability of thermal barrier coatings, " *Progress in Materials Science*, vol. 46, pp. 505-555, 2001.

[35] M. Okazaki, S. Yamagishi, M. Sakaguchi, S. Rajivgandhi, "Specific failures of Superalloys with thermal barrier coatings subjected to thermo-mechanical fatigue loadings with a thermal gradient in a simulated combustion environment, " *Superalloys conference,* 2012.

[36] D. Arrell, M. Hasselqvist, C. Sommer, and J. Moverare, "On TMF damage, degradation effects, and the associated T-Min influence on TMF test results in gamma/gamma' alloys, *Superalloys conference*, pp.291-294, 2004.

[37] R.C. Reed, "The superalloys : fundamentals and applications, "*Cambridge University Press*, 2006.

[38] A. Raffaitin, D. Monceau, E. Andrieu, and F. Crabos, "Cyclic oxidation of coated and uncoated single-crystal nickel-based superalloy MC2 analyzed by continuous thermogravimetry analysis," *Acta Mater.*, vol. 54, no. 17, pp. 4473–4487, Oct. 2006.

[39] R. Giraud, J. Cormier, Z. Hervier, D. Bertheau, K. Harris, J. Wahl, X.Milhet, J. Mendez, A. Organista, " Effect of the Prior Microstructure Degradation on the High Temperature/Low Stress Non-Isothermal Creep Behavior of CMSX-4 Ni-Based Single Crystal Superalloy, " *Superalloys conference,* at Seven Springs, PA, USA, edit TMS, 2012.

[40] J. Cormier, M. Jouiad, F. Hamon, P. Villechaise, X. Milhet, " Very high temperature creep behavior of a single Ni-based superalloy under complex thermal cycling conditions, " *Phil. Mag. let.* vol. 90, no. 8, pp. 611-620, 2010.

[41] J. Cormier, X. Milhet, J. Mendez, " Non-isothermal creep at very high temperature of the nickel based single crystal superalloy MC2, " *Acta Materialia*, vol. 55, pp. 6250-6259, 2007.

[42] J.B. le Graverend, A. Jacques, J. Cormier, O. Ferry, T. Schenk, J. Mendez, " Creep of e nickel-based single cristal superalloy during very high temperature jumps followed by synchrotron x-ray diffraction, " *Acta Materialia*, vol. 84, pp. 65-79, 2015

[43] C. Schwalbe, J. Cormier, C.N. Jones, E. Galindo-Nava, C. Rae, "Investigating the Dislocation-Driven Micro-mechanical Response Under Non-isothermal Creep Conditions in Single-Crystal Superalloys, " *Metallurgical and Materials Transactions A*, vol.49A, pp. 3988-4002, 2018.

[44] B. Larrouy, P. Villechaise, J. Cormier, O. Berteaux, " Grain boundary–slip bands interactions: Impact on the fatigue crack initiation in a polycrystalline forged Ni-based superalloy, " *Acta Materialia,* vol. 99, pp. 325-336, 2015.

[45] P. Villechaise, J. Cormier, T. Billot, J. Mendez, " Mechanical Behavior and Damage Processes of Udimet 720Li: Influence of Localized Plasticity at Grain Boundaries, " *Superalloys conference,* at Seven Springs, PA, USA, edit TMS, 2012.

[46] F. Riallant, " Modes d'endommagement à chaud du système AM1/NiAlPt/BT EBPVD : impact de la plasticité et interactions revêtement-substrat, " PhD thesis, ISAE-ENSMA, 2014.

[47] Y. Xingfu, T. Sugui, D. Hongqiang, Y. Huichen, W. Minggang, S. Lijuan, C. Shusen, " Microstructure evolution of a pre-compression nickel-base single crystal superalloy during tensile creep, " *Materials Science and Engineering: A*, vol. 506, no. 1-2, pp. 80-86, 2009.

[48] C. Petroral, J. Ilavsky, H. Wang, W. Porter, R. Trice, " Microstructural evolution of 7 wt.% Y2O3–ZrO2thermal barrier coatings due to stressrelaxation at elevated temperatures and the concomitant changes inthermal conductivity, " *Surf. Coat. Technol.*, vol. 205, pp. 57-65, 2010.

[49] C. Petorak, R. Trice, " Effect of heat-treatment on stress relaxation behavior of plasma-sprayed 7 wt.% Y2O3–ZrO2 stand-alone coatings, " Surf. Coat. Technol., vol. 205, pp. 3218-3225, 2011.

[50] T. Beck, O. Trunova, R. Herzog, L. Singheiser, "TBCs for Gas Turbines under Thermomechanical Loadings: Failure Behaviour and Life Prediction, " *European Physical Journal conference,* vol. 33, 2012.

[51] R. Subramanian, Y. Mori, S. Yamagishi, and M. Okazaki, "Thermo-mechanical Fatigue Failure of Thermal Barrier Coated Superalloy Specimen," *Metall. Mater. Trans. A*, vol. 46, no. 9, pp. 3999–4012, 2015.

[52] M. Bartsch, B. Baufeld, S. Dalkiliç, L. Chernova, M. Heinzelmann, " Fatigue cracks in a thermal barrier coating system on a superalloy in multiaxial thermomechanical testing, " *Intern. J. of Fatigue,* vol. 30, no. 2, pp. 211-218, 2008.

[53] S. Kyaw, A. Jones, M.A.E. Jepson, T. Hyde, R.C. Thomson, " Effects of three-dimensional coating interfaces on thermo-mechanical stresses within plasma spray thermal barrier coatings," *Materials and design,* vol. 125, pp. 189-204, 2017.

[54] P. Shalka, K. Skamecka, J.Pokluda, L.Celko, " Finite element simulation of stresses in a plasma-sprayed thermal barrier coating with a crack at the TGO/bond-coat interface, " *Surface and coatings technology,* vol. 337, pp. 321-334, 2018.

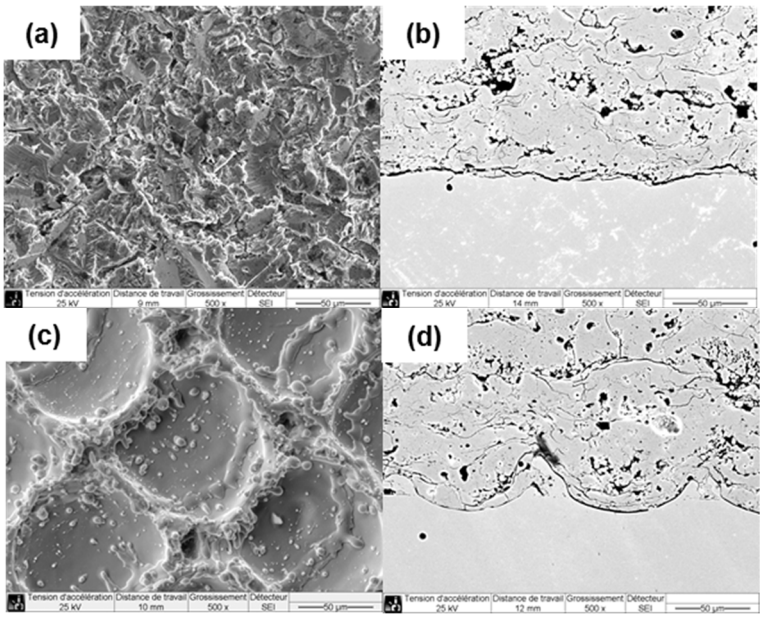

Figure 1: Top-view and cross-sections of grit-blasted (a, b) and laser textured (c, d) substrates

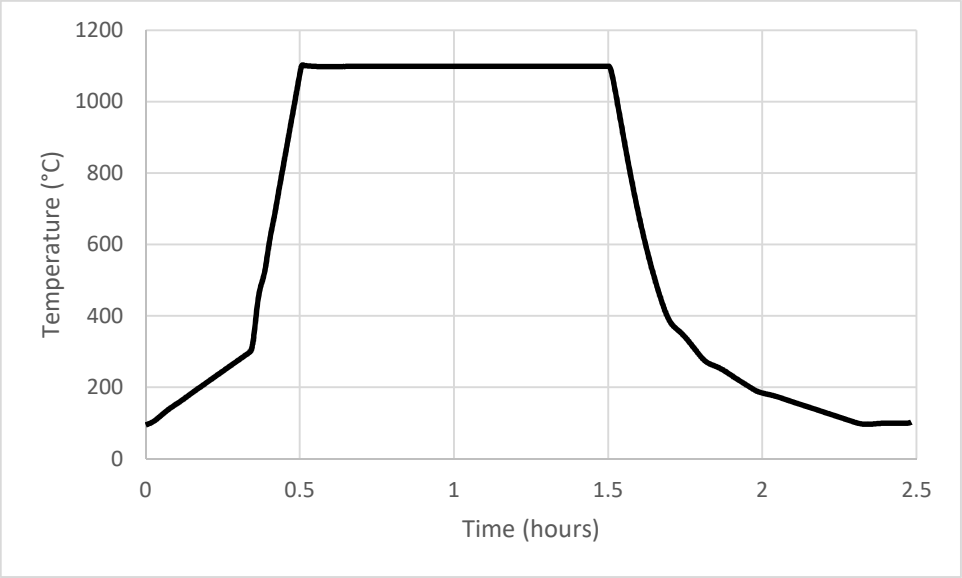

Figure 2: Thermal cycle applied during oxidation tests

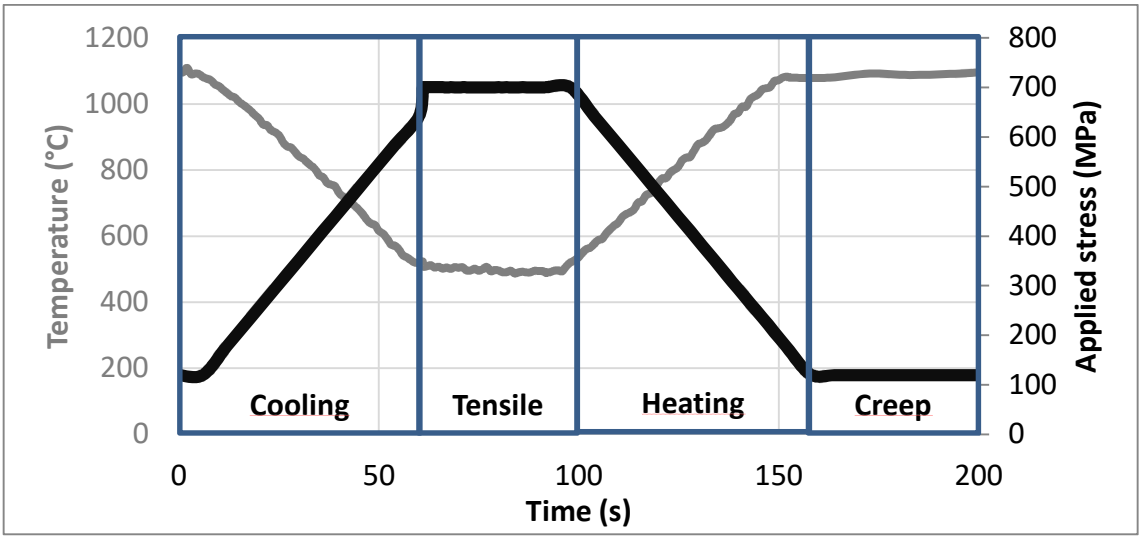

Figure 3: Applied out-of-phase TMF cycle at the leading edge of specimens - Temperature and applied stress function of time

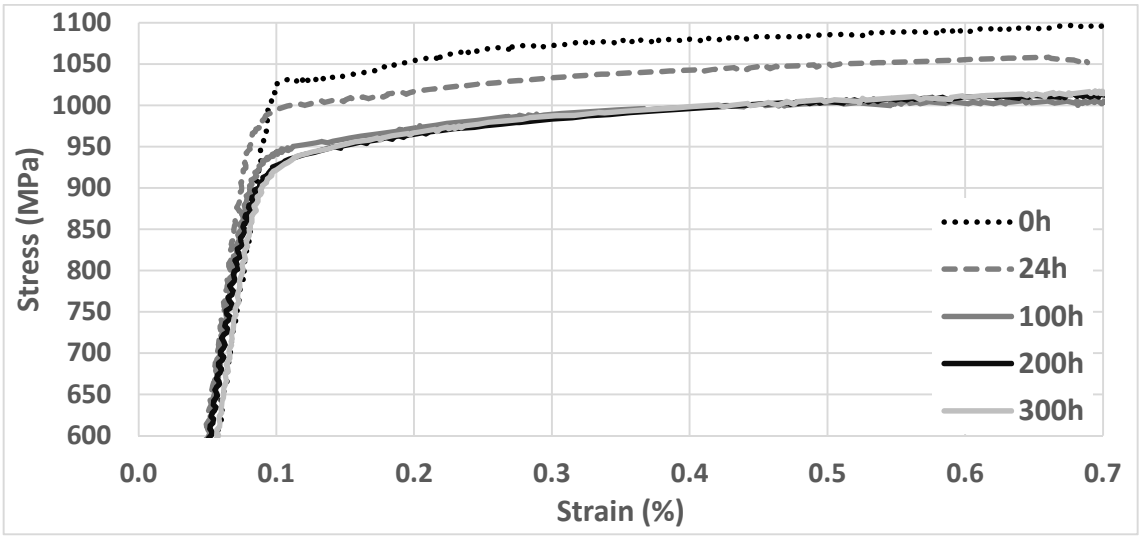

Figure 4: Tensile behavior at 500°C/10^{-3} s^{-1} after 0, 24, 100, 200 and 300h prior thermal-aging treatments

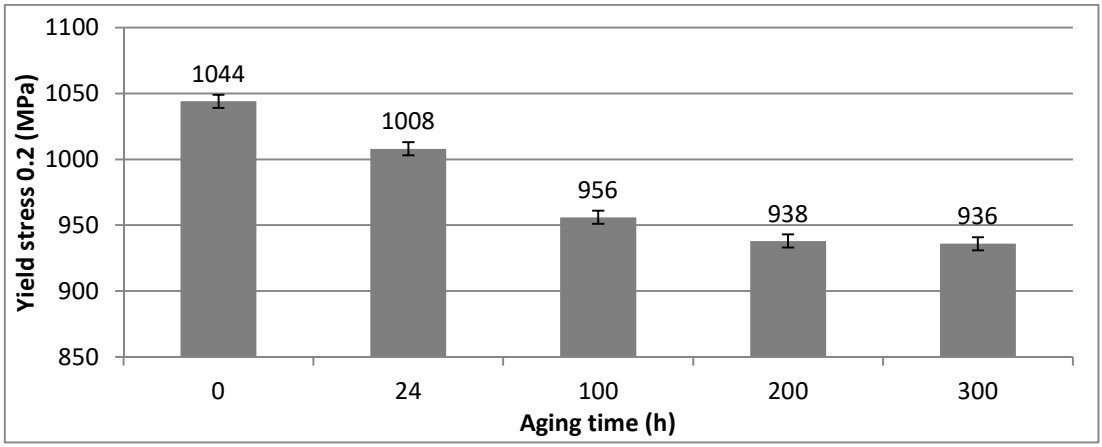

Figure 5: Yield stress at 500°C/10^{-3} s^{-1} evolution as of the over-aging time at 1100°C for the AM1 superalloy

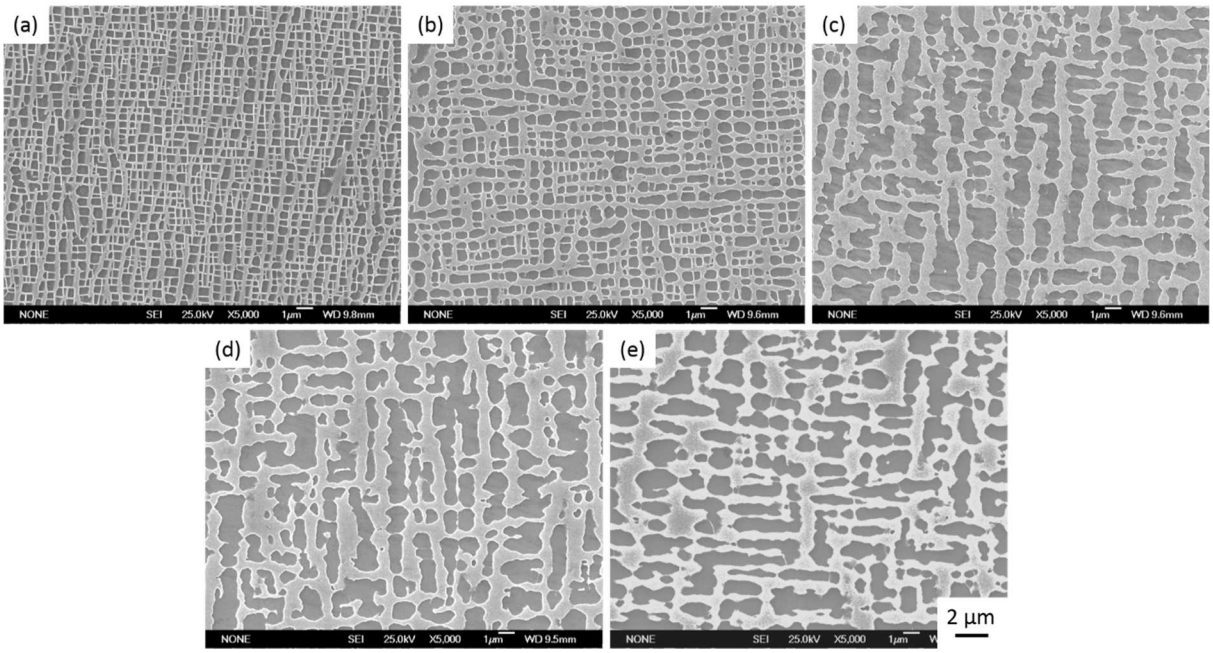

Figure 6: γ/γ' microstructure in primary dendrite arms of AM1 single crystal superalloy: (a) in the as-received state , (b) after 24h at 1100°C, (c) after 100h at 1100°C , (d) after 200h at 1100°C, (e) after 300h at 1100°C

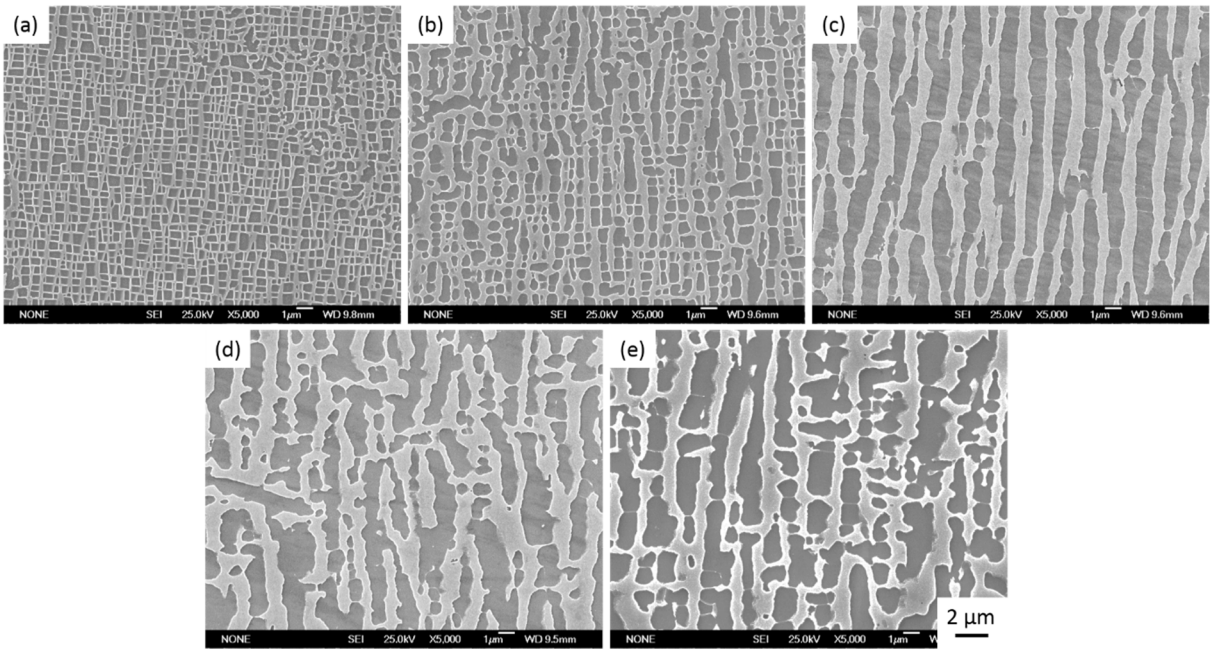

Figure 7: γ/γ' microstructure in interdendritic spacings of AM1 single crystal superalloy: (a) in the as-received state, (b) after 24h at 1100°C, (c) after 100h at 1100°C , (d) after 200h at 1100°C, (e) after 300h at 1100°C

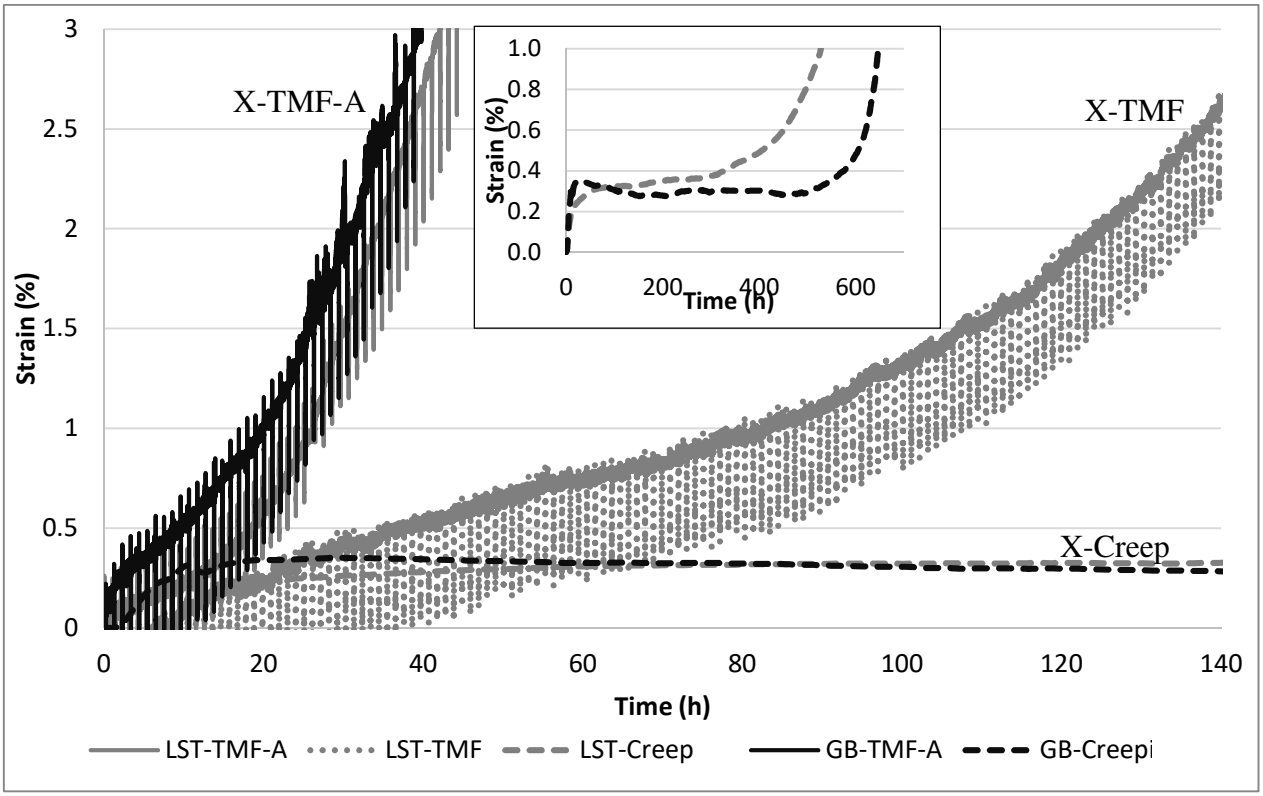

Figure 8: Creep and OP-TMF behavior. The creep behavior over all the tests duration is provided in insert.

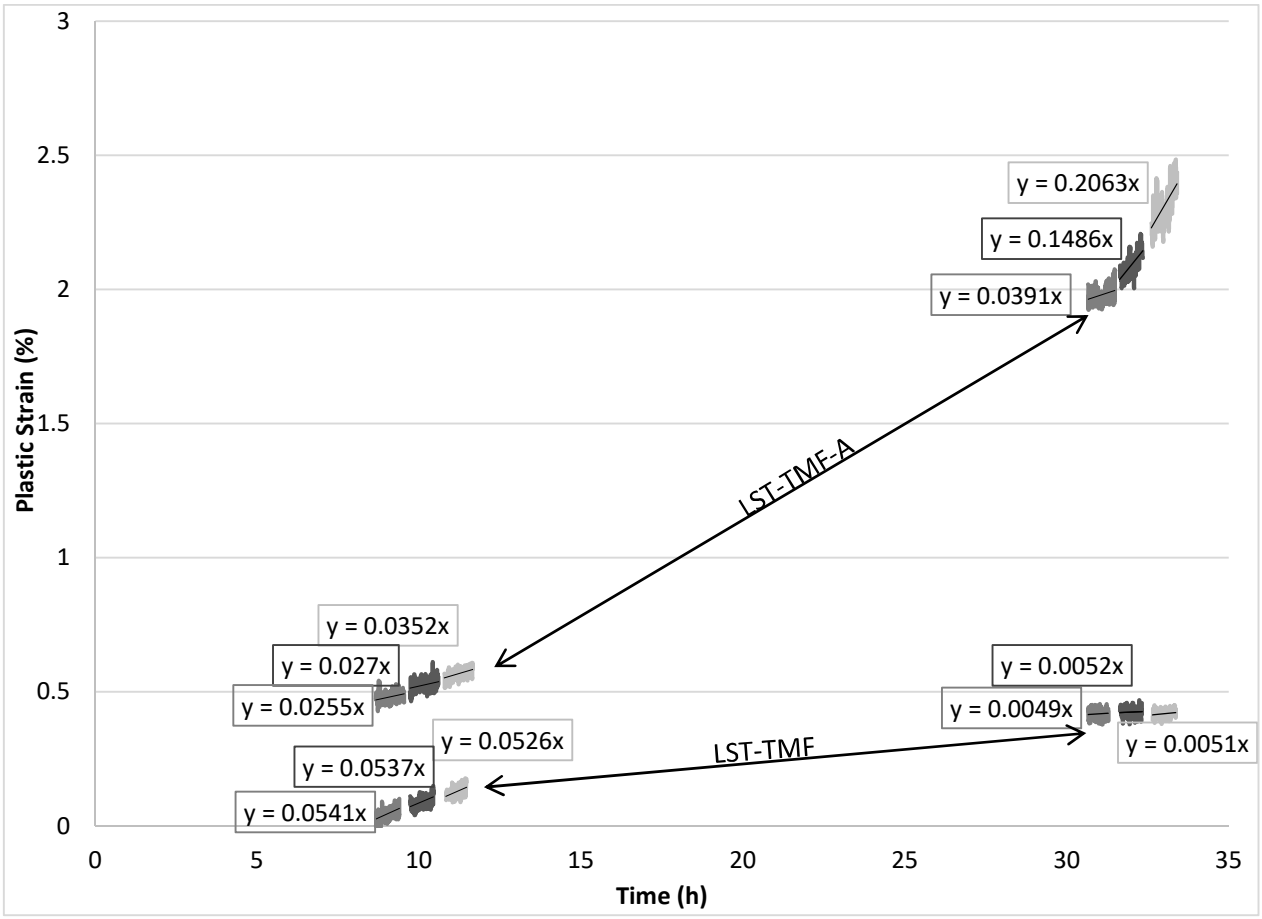

Figure 9: Total strain evolution for selected cycles of LST-TMF and LST-TMF-A tests

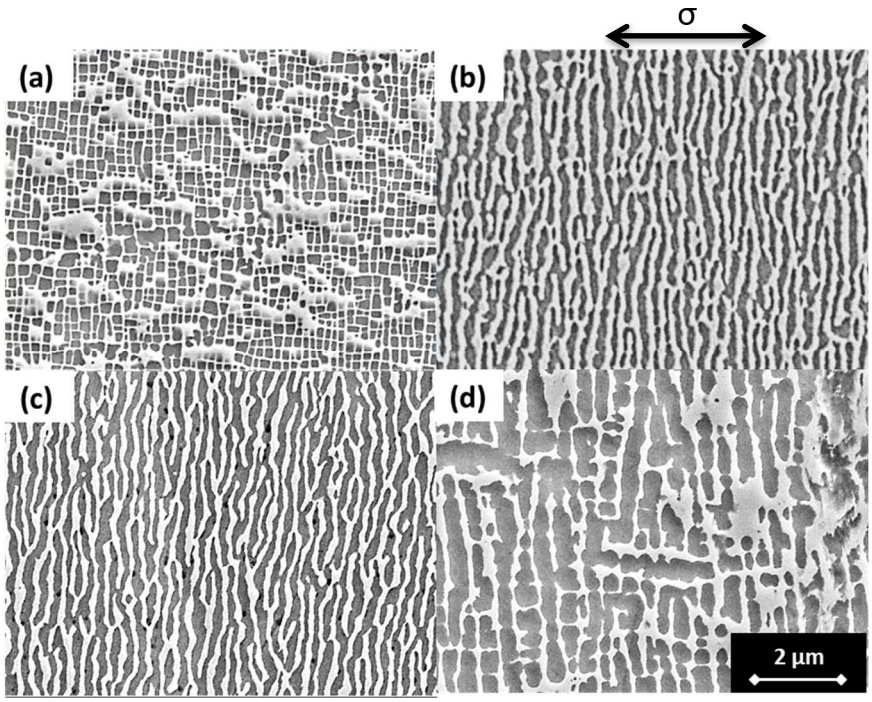

Figure 10: SEM observations of the γ/γ' microstructure in primary dendrite arms (a) in as-received specimens, (b) after creep tests, (c) after a TMF test without any prior over-aging and (d) after over-aged TMF test (horizontal applied stress)

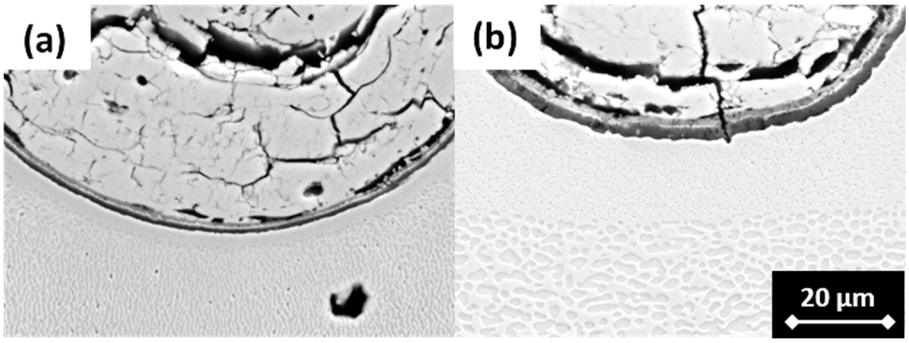

Figure 11: Cross-sections of a) LST-TMF and b) LST-TMF-A samples in pattern

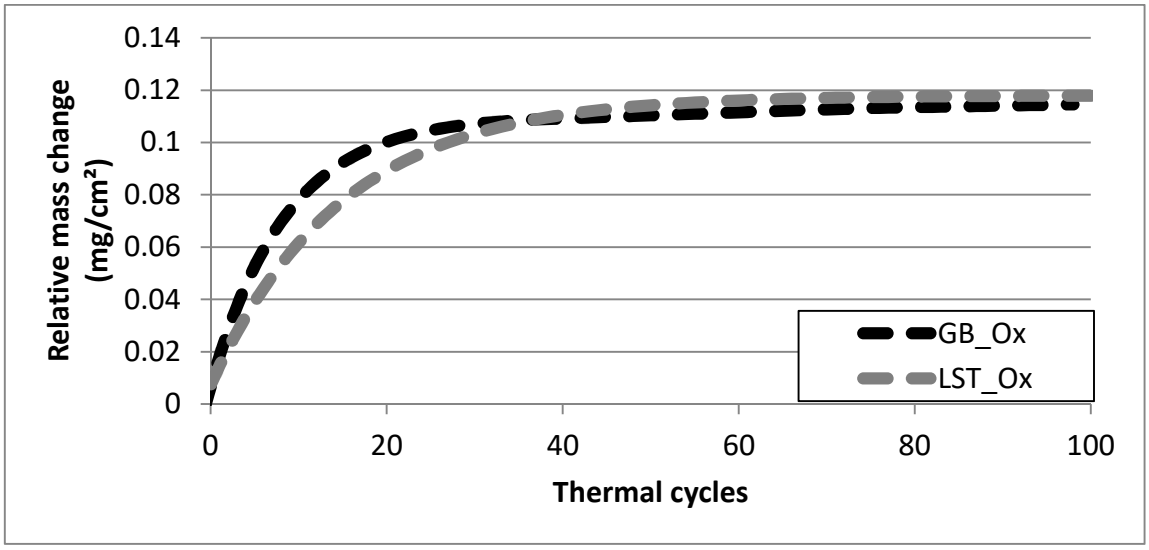

Figure 12: Relative mass change as a function of the number of thermal cycles for isothermal and thermal cycling tests – Grit-blasted (GB) and laser textured samples – errors of 0.0002 $mg.cm^{-2}$

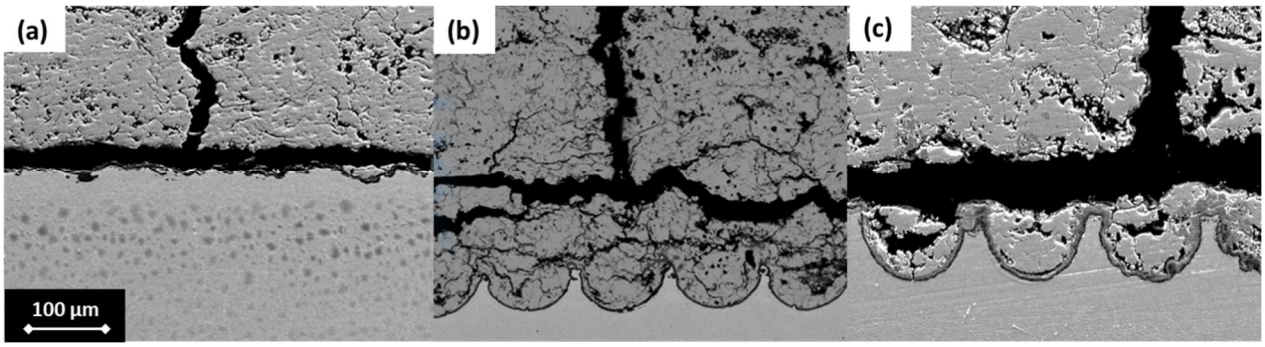

Figure 13: Top coat damage mechanism observed in a) GB-TMF b) LST-TMF and c) LST-TMF-A specimens

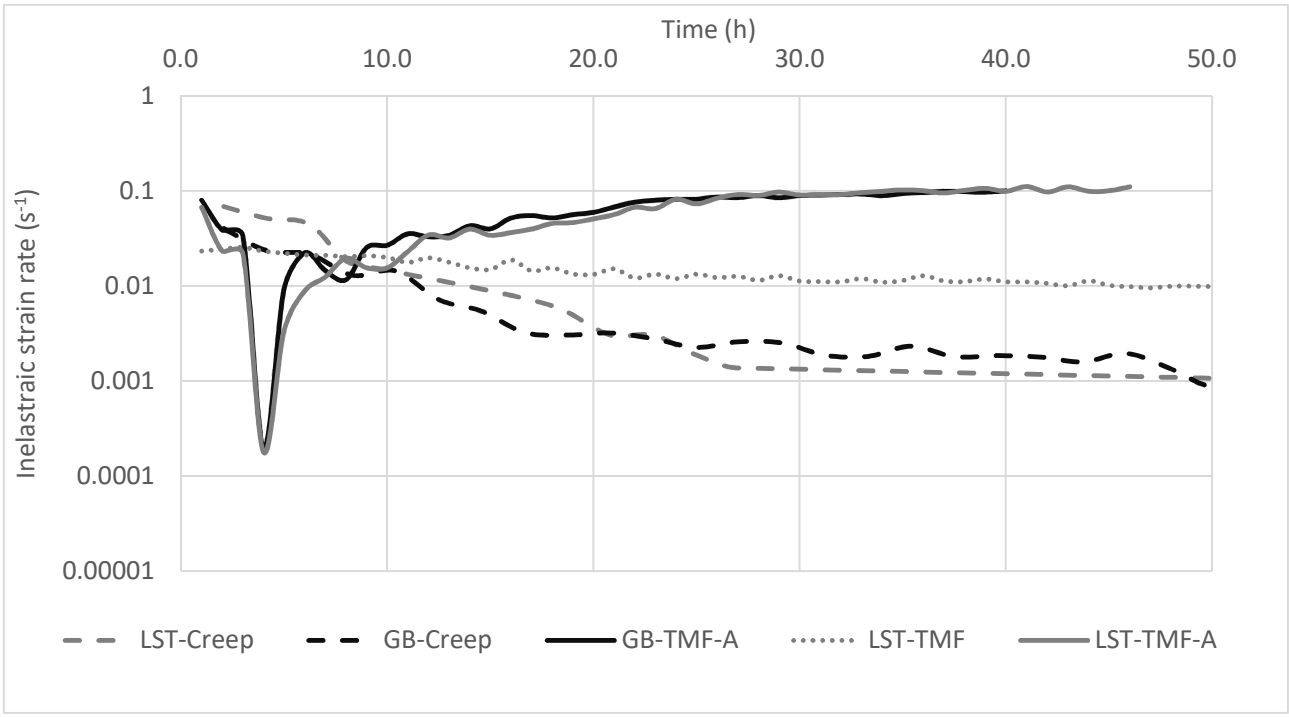

Figure 14: Evolution of the inelastic strain rate as a function of time during creep and TMF tests

Table 1: AM1 chemical composition (wt pct.)

Ni	Co	Cr	Mo	W	Al	Ti	Ta	Hf
Bal.	6.6	7.5	2.0	5.5	5.2	1.2	7.9	0.04

Table 2: Thermal spray parameters for top coat

Primary gas flow rate [slpm]	Ar	44
	H_2	13
Spray Distance[mm]	120	
Arc current [a]	630	
Powder Feeding rate[g/mm]	23	
Carrier gas flow [L/min]	3.4	
Angle injection [°]	90	

Table 3: Tensile, Oxidation, creep and Out-of-Phase TMF tests performed in this study for grit-blasted (GB) and textured (LST) samples. X accounts for either GB or LST specimens.

Samples (X: GB/LST)	Stages	Stress loading (MPa)	Temperature loading (°C)	Prior-thermal aging
Tensile	-	-	500	0/300h – 1100°C
X-Ox	1h/30sec	-	1100/100	-
X-Creep	(1%)	120	1100	-
X-TMF	1h/30sec	120/700	1100/500	-
X-TMF-A	1h/30sec	120/700	1100/500	200h-1100°C

Table 4: Ultimate tensile strength and ductility (at 500°C/10^{-3} s^{-1}) as a function of the aging time at 1100°C for the AM1 superalloy

Aging time (h)	0	24	100	200	300
UTS (MPa)	1098	1053	1005	1015	1015
Ductility (%)	6.2	6.1	6.7	6.5	8.5

Table 5: Oxide thickness (in µm) after 50 and 150 oxidation cycles and after TMF tests (±0.15 µm) * debonded top coat

Cycle number	GB-Ox	LST-Ox	GB-TMF-A	LST-TMF-A	LST-TMF
50	2.7	2.9	3	3.2	-
150	*	3.4	-	-	3.6